Evaluation and Current-Response-Based Identification of Insulation Degradation for High Utilized Electrical Machines in Railway Application

Clemens Zoeller, Markus A. Vogelsberger, Robert Fasching, Werner Grubelnik, *Member, IEEE*, and Thomas M. Wolbank, *Member, IEEE*

***Abstract*—The demand for condition monitoring systems to prevent a breakdown of electrical machines is continuously increasing. A failure or collapse of the insulation is one of the main reasons for a machine outage, both in the field of high-voltage machines as well as low voltage. Especially at inverter-fed motors, several kinds of stresses due to parasitic phenomena exist and cause decrease of the insulation lifetime. With the method proposed, the evaluation of the stator insulation health condition of inverter-fed motors is possible by analyzing the current sensors transient response after inverter voltage step excitation. The analysis of the transient signal portion gives evidence of a possible change in the insulation system by comparison of the characteristics with the known pattern of the healthy machine transient signal portion. Tests are performed on a 1.4-MW induction machine designed for traction applications. By the availability of taps accessible on the machine terminal, different scenarios to emulate winding insulation degradation are conducted. Additionally, in order to investigate insulation degradation characteristics of the used insulation materials, accelerated aging procedures are applied on specially manufactured stator slot models with form-wound coils. These stator test segments have been aged by different accelerated aging cycles until the failure of the insulation is determined by voltage exposure tests. With additional nondestructive diagnostic measurements, e.g., dissipation factor ($\tan\delta$), capacitance, the correlation between these indicator values, the results of the proposed method, and the degradation of the insulation strength until a breakdown are investigated.**

***Index Terms*—Aging, fault diagnosis, induction motors, insulation testing, pulse inverters, traction motor drives.**

Manuscript received July 1, 2016; revised November 4, 2016 and December 22, 2016; accepted December 31, 2016. Date of publication January 31, 2017; date of current version May 18, 2017. Paper 2016-EMC-0459.R2, presented at the 2015 IEEE 10th International Symposium on Diagnostics for Electrical Machines, Power Electronics, and Drives, Guarda, Portugal, Sep. 1–4, and approved for publication in the IEEE TRANSACTIONS ON INDUSTRY APPLICATIONS by the Electric Machine Committee of the IEEE Industry Applications Society. This work was supported by the Austrian Research Promotion Agency (FFG) under Project 838478; in part by ISOVOLTA Austria; in part by Bombardier Transportation Switzerland, Ltd; and in part by Bombardier Transportation Austria GmbH.

C. Zoeller is with the Technische Universitat Wien Fakultat fur Elektrotechnik und Informationstechnik, Wien 1040, Austria (e-mail: clemens.zoeller@tuwien.ac.at).

M. A. Vogelsberger is with Bombardier Transportation Austria GmbH, Vienna 1220, Austria (e-mail: markus.vogelsberger@rail.bombardier.com).

R. Fasching and W. Grubelnik are with Isovolta AG, Wiener Neudorf 2355, Austria (e-mail: Robert.Fasching@Isovolta.com; Werner.Grubelnik@isovolta.com).

T. M. Wolbank is with the Department of Energy Systems and Electrical Drives, Vienna University of Technology, Vienna 1040, Austria (e-mail: thomas.wolbank@tuwien.ac.at).

Color versions of one or more of the figures in this paper are available online at http://ieeexplore.ieee.org.

Digital Object Identifier 10.1109/TIA.2017.2661718

NOMENCLATURE

C	Capacitance.
f	Frequency.
fS	Sampling frequency.
f_i	Discrete frequency.
ISI	Insulation state indicator.
k	Identifier of consecutive measurement.
n	Observation frequency range.
PD	Partial discharge
RMSD	Root mean square deviation.
SISI	Spatial insulation state indicator.
t	Time.
Un	Nominal voltage.
$x1$	Signal 1.
$x2$	Signal 2.
$Y\mathrm{con}$	Frequency spectrum of condition measurement.
Y_{ref}	Frequency spectrum of reference measurement.

Subscripts

$c-c$	Coil-to-Coil.
g	Global.
p, ph	Phase.
$ph-ph$	Phase-to-phase.
$t-t$	Turn-to-turn.
$w-gnd$	Winding-to-ground.
L1, L2, L3	Machine phase.

I. INTRODUCTION

THE ELECTRICAL insulation for rotating machines is one of the most important parts, although it is often seen as ballast that delivers no share on the energy conversion inside the machine. However, a weak insulation system could not guarantee the continuous operation without an outage over decades. The strength of the insulation is gradual degraded during operation of the machine through different combined stresses, e.g., thermal, electrical, mechanical, and environmental influences [1]. Today's estimation of the insulation condition and the remaining life of the insulation of a machine is evaluated with empirical methods based on extensive tests and dielectric measure-

ments, like capacitance [3], dissipation factor [4], and insulation resistance measurements [5], which deliver integral diagnostic of the insulation strength. With the partial discharge test locally limited defects can be investigated [6], [7]. These tests often demand the experience of the examiner. Principally, monitoring methods can be classified in off- or on-line techniques. In case of off-line tests the machine is partly disassembled from the drive system and requires by definition a short outage, e.g., [8]–[10]. In contrast, online tests are applied during operation, although, in some cases the condition of the machine operation is changed to enable a correct diagnose. In [11]–[14], the presented online techniques require additional signal injection sources, which in turn require additional coupling and decoupling equipment to enable the evaluation of the test signals. The methods presented in [15], [16] to diagnose insulation problems are better suited for detection of an existing fault than detecting an imminent degradation of turn-to-turn insulation of the stator winding. In [17], many condition monitoring and fault diagnosis methods have been summarized.

Investigations published by different authors showed the effects at deterioration of insulation systems for high-voltage rotating machines as a function of test voltage [18], [19]. The results show that one reliable parameter for the estimation of insulation degradation is the measured capacitance. According to Perisse *et al*., changes of the turn–turn capacitances resulting from stress through thermal cycling is detectable. The insulation degradation process is usually slowly developing, first starting with the deterioration of the turn-to-turn insulation and finally leading to higher severity faults like phase-to-phase or phase-to-ground, respectively, until a breakdown of the insulation.

The following paper is divided into two main parts. First the investigations and procedure of the accelerated aging test of stator winding coils are described. In the second part, the proposed monitoring technique for stator insulation deterioration in traction motors is presented.

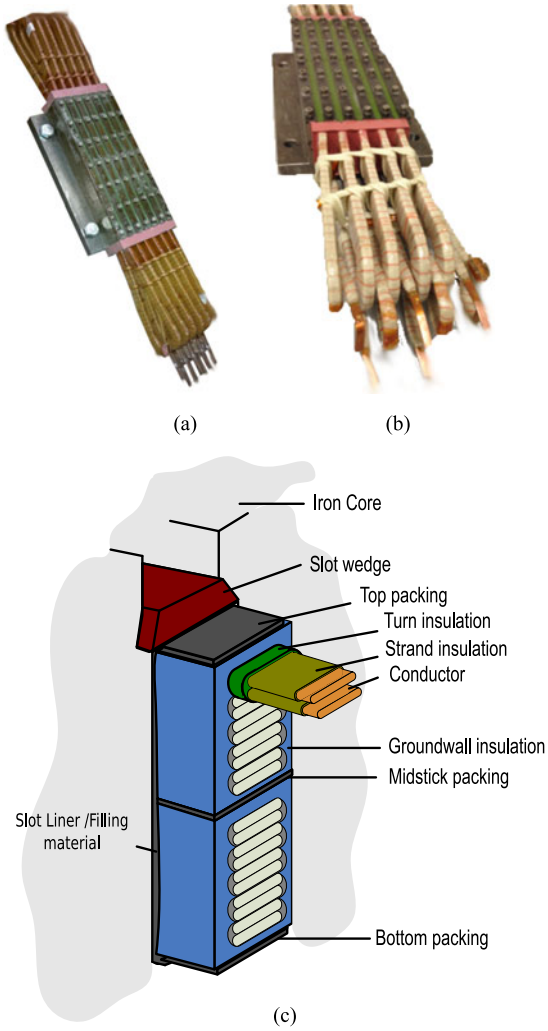

Fig. 1. (a) Type I and (b) type II stator slot specimens "formette." (c) Slot structure and insulation components.

II. Form Wound Coil Test Setup

In this section, a short description of the construction details and used insulation materials of the form wound coils is given. For the investigations of this work, in the following the generic name "formette" is applied to test models coming within the scope of this procedure that are modeled and available for the aging tests and analyzes. A formette consists of a massive iron body with five slots for top and bottom coils. A figure of the formettes is depicted in Fig. 1(a) and (b). A test setup is built out of several serially connected coils. The coil span has been changed from the machine design so that the forward and backward conductors of a coil are placed in adjacent slots. The detailed structure of a slot including the copper conductors and insulation is depicted in Fig. 1(c). A short description of the insulation system, starting from the inner conductor to outward explains the properties and nature of the insulation system applied. In the scheme of the insulation system, it is observable that strand and turn insulation are separated. The winding conductor is frequently split in two single subconductors, both separated by the strand insulation. These subconductors are easier to bend by keeping a constant cross section. Additionally, the eddy current losses due to the smaller cross section are reduced. Typically, the strand insulation is very thin, since the voltage drop between the strands is very low. An occurring strand short circuit probably would not cause winding failure in the first stage, but increase the stator winding losses and cause local temperature increase by circulating currents. The conductor insulation is often made of enamel and glass covering.

The turn insulation can be considered as an important insulation component, although many manufacturers try merging the turn and strand insulation to one single component [1]. Assuming an almost equal voltage distribution along the coils from phase terminal to neutral, the voltage drop at medium voltage machines can reach up to several hundred volts. A failure in this insulation component will result in progressive deterioration and fast propagation to several other components. High transient voltages, as occurring at inverter-fed operation, additionally stress the turn insulation and in the worst case, may puncture the insulation.

The groundwall insulation separates the conductors from the stator core. Today's insulation systems of medium voltage traction motors consist of mica tapes, polyimide film/glass-fiber, woven glass tapes, and impregnating resins for the groundwall

insulation. This is one of the main components of the system. In case of a crack or discontinuity a current flow from copper conductor to iron core is possible and may damage the stator core. Especially, groundwall insulation faults close to neutral are hardly detectable. Materials used as slot liners are typically composite materials, e.g., laminates based on a compound polyimide foil, fiberglass and aramid.

A. Test Procedure

The test procedure is established in accordance with the IEEE standard 1776 -2008 [21]. On an accelerated basis, thermal deterioration effects are analyzed by conducting heat exposures in repeated cycles. Thermal aging by heating the formettes to a defined temperature above the maximum approved level plays an important role on insulation degradation. A temperature increase above the threshold of the used insulation materials leads to loss of mechanical strength, as well as a reduction of electrical breakdown voltage.

Additionally to the thermal cycles the formettes are exposed in a sequence to mechanical stress and moisture exposure by humidification and water immersion for sealed systems. After mechanical stress and moisture exposure and at the end of the water immersion a withstand voltage test is done to detect cracks inside the insulation. The procedure is repeated until the voltage tests identify a failure of the insulation system.

Due to the recommended number of ten exposure cycles before failure for each formette, a small number of single formwound coils of the same insulation system were subjected to extreme aging in a prestudy with a temperature $>$ 300 °C to estimate a suitable exposure setup (insulation class 200). Based on the experience of the prestudy test coils and the results it was decided that the thermal aging of the four formettes is separated into two groups with two different aging temperatures (ϑ_1 and ϑ_2) for different thermal stress intervals (denoted "Cycle A" and "Cycle B"). As can be seen in Fig. 2, two different aging cycles are defined and for two formettes cycle A is applied and for the other two formettes cycle B. This should enable that the most experience is generated through the collected data.

At first, the thermal evaluation cycle starts with the mechanical stress by mounting the formettes on the vibrating table at 50 Hz oscillating motion and 1.5 g for 60 min. Second, the insulation condition is estimated and quantified with capacitance and dissipation factor as can be seen in the following sections. In step three, the formettes are placed in the humidity chamber for 48 h at 95–100% relative humidity followed by step four, the first voltage exposure with 10 min at 5 kV.

After the first voltage exposure, the formettes are immerged into water for 30 min (step five) with subsequent second voltage exposure with 1.15 U_N for 1 min (step six). After cleaning the formettes with tap water and drying overnight (step seven), the heat exposure is done with ϑ_1 for 14 days (cycle A) and ϑ_2 for 4 days (cycle B), respectively, as the final step. All steps are repeated until a voltage exposures test fails. After passing the voltage test the insulation state of the formette/coil is denoted state "X", where "X" refers to the number of cycles passed.

The multifactorial aging tests started during the establishing of this paper.

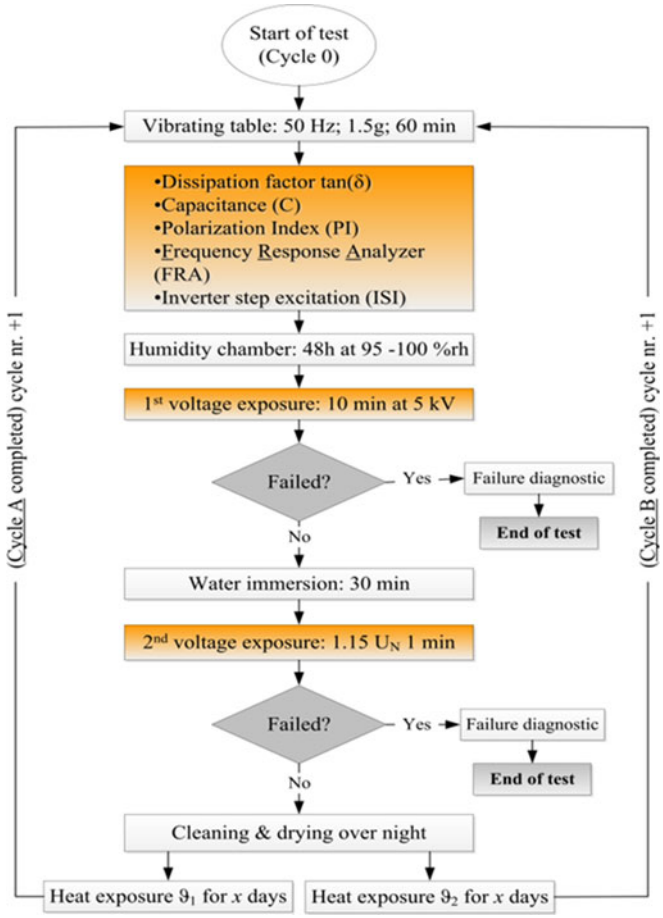

Fig. 2. Thermal aging cycle.

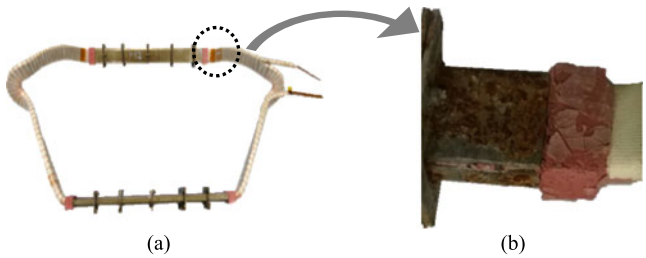

Fig. 3. (a) Pilot coil and (b) effect of four thermal cycles.

B. Results of Test Coil Investigations

Before starting the test of the four formettes type II, single test coils and one type I formette were exposed to accelerated aging to estimate the duration of the test series. Capacitance, $\tan\delta$ and polarization index measurements were conducted in both cases. The thermal evaluation cycles are conducted but with a heat exposure temperature of 310 °C for 24 h. In Fig. 3(a), the test coil is depicted and in (b) the effect of four thermal cycles is analyzed on the slot closure of the coil. After thermal cycle 4 and 5, respectively, an electric breakdown was detected on the winding overhang on two different coils.

Regarding the measurement setup, especially in case of the dissipation factor, various techniques like usage of guard electrodes are recommended in [4] to minimize the measurement

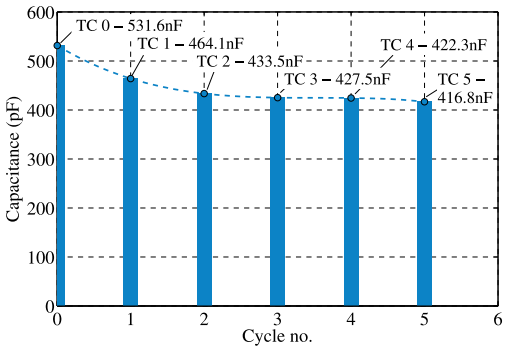

Fig. 4. Decrease of prestudy test coil capacitance about 20% within five thermal cycles.

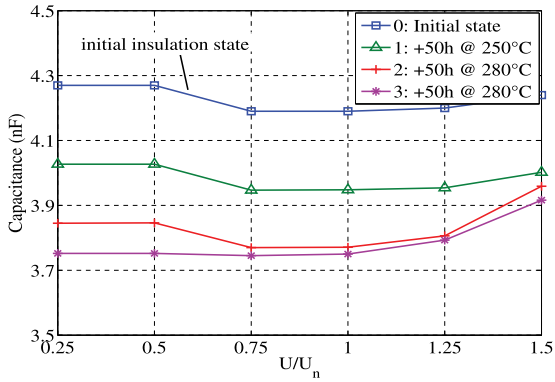

Fig. 5. Dissipation factor tan(δ) of the formette type I.

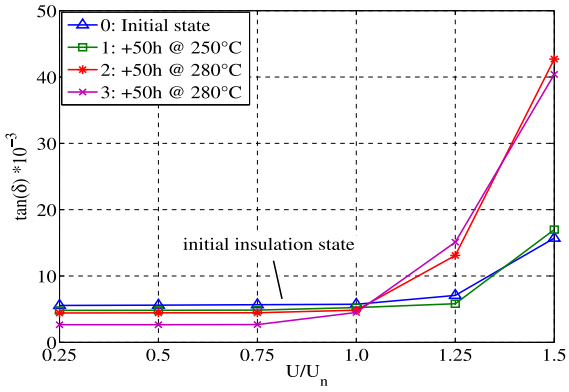

Fig. 6. Capacitance of the formette type I.

errors. The slot closure mainly serves to prevent moisture from penetrating into the slot. However, the dissipation factor and capacitance measurements were conducted with and without wrapped metal foil and guard electrodes to analyze the influence of the measurement setup. First case demands that the foil is tightly applied with minimized voids and air pockets that can affect the measurement. Due to the low test voltages of < 5 kV and the omission of a semiconductive field grading, the deviation between guarded and unguarded measurement with respect to dissipation factor, especially the capacitance seems to be negligible for that setup. The results showed no significant differences with or without the guard ring. By examining the figure of the formettes (see Fig. 1), it is observable that placing the guard electrodes with required distance of about 2–3 mm from the end of the stress grading slot coating was not possible. Thus, to ensure the same measurement setup for all specimens, the guard electrodes were omitted in all investigations without loss of accuracy or significance. Therefore, it was decided to measure the dissipation factor and capacitance without guard rings.

Before the measurement is done, a conditioning test is performed to stabilize the dissipation factor measurement. A conditioning voltage is selected and the influence of the conditioning was observed at several test measurements and more stable results were determined with the conditioned coils especially at lower voltages.

In Fig. 4, the capacitance change after five thermal cycles at nominal voltage is depicted.

The results show the decrease of the capacitance about 20% within five thermal cycles.

C. Results of Formette Type I Investigations

The specimen formette "type I" was only thermally aged. Heat exposures with different duration were applied. The operating state before the ageing process, denoted "*0: initial state*", is analyzed by evaluating the dissipation factor and capacitance. The first heating process, denoted with "*1: +50 h @ 250 °C*" was realized by injecting a high dc current with up to 160 A to heat up the coils and iron. This emulates a realistic heat source from the copper of the coils, like it occurs in practical application. Additionally, heating resistors are used on the iron part of the formette to accelerate the procedure. Afterwards, two further thermal exposure periods with in each case 50 h at 280 °C are applied to the formette. After each heat exposure the dissipation factor and capacitance is evaluated.

In Fig. 5, the measured dissipation factor as a function of test voltage is recorded. The values are slightly decreasing for test voltages below nominal voltage in case of all three states. This occurs mostly due to drying and post curing of uncured resin sections of the insulation during the first cycles. These changes indicate a decrease in the sum of the polarization and conducting losses within the insulation.

A rise of the dissipation factor tan(δ) with test voltage from nominal voltage to 1.5 U_n is observable with increasing number of aging cycles. The high tan(δ) values in the upper test voltage range above nominal voltage are mainly caused by delamination and voids within the main insulation. These partial discharge activities are leading to higher ionization losses. These dissipation factor "tip-up" or increase with voltage as a result of internal discharges has been a sort of qualitative indication of insulation integrity.

In Fig. 6, the capacitance value of the complete winding measured against ground is depicted in case for the initial value and after the applied three cycles. The decrease of the initial capacitance value is observable as also is the voltage dependency of the measurement. Again the reason is dedicated to delamination caused by deterioration through thermal aging resulting in an increasing number of voids at the groundwall. Through

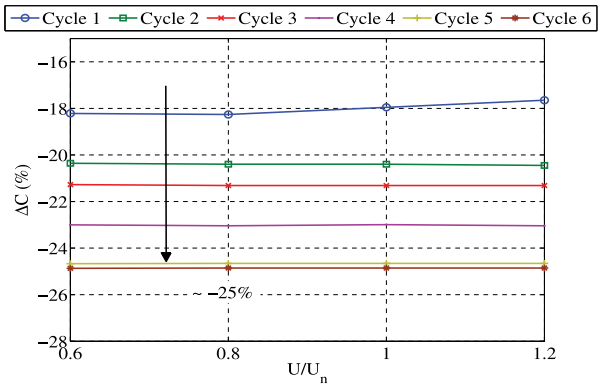

Fig. 7. Normalized change in percentage of capacitance of formette type II – after six thermal aging cycles.

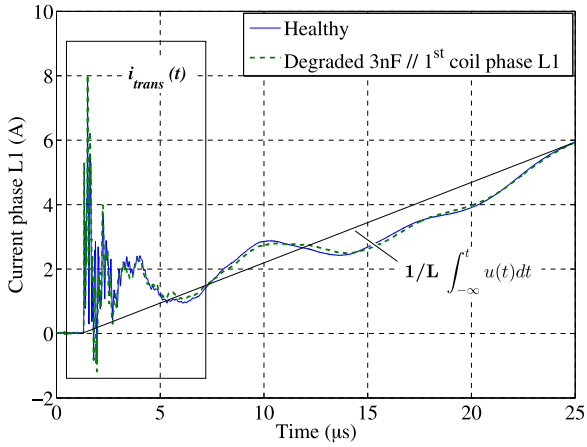

Fig. 8. Current response after step excitation, healthy machine state (solid blue), and degraded insulation (dashed green).

the lower dielectric constant of air (∼1) compared to typical insulation materials, which is about 3–5, the average dielectric constant decreases and as a consequence the capacitance of the specimen.

The total capacitance value is influenced at low voltage levels by solid insulation and cavities. At higher voltage levels, above the corona starting voltage, the capacitance values are increasing and only the solid insulation is influencing the measurement, because the voids have been shorted by partial discharge.

D. Results of Formette Type II Investigations

The thermal aging cycles, as described in Fig. 2, are applied to the four formettes of type II. In Fig. 7, the mean values of the capacitance and dissipation factor measurements are depicted. The left subfigure shows the normalized change of the capacitance values between the actual cycle C_x and the initial state C_0 ($\Delta C = (C_x - C_0)/C_0$) for different voltage levels. After six aging cycles, the formettes failed the withstand voltage tests. This results in a maximum capacitance change of about 25%.

The results of these experiments provide information about the behavior and changes of the electrical properties of a deteriorated winding insulation system. Through better understanding, the results help to improve the developed insulation monitoring procedure. In Section III, the proposed stator insulation monitoring method for inverter fed machines is presented.

III. Insulation Monitoring Method

An inverter delivers the ability to control the angular velocity of the rotor shaft by supplying the stator winding with voltage of variable frequency/magnitude using the pulse width modulation (PWM). The steep voltage edges induced by the PWM output of the inverter produce surges at the machine terminal [22], [23]. The insulation system of the machine suffers under these transient overvoltages. The short rise time of newer upcoming inverter semiconductor technologies, e.g., SiC or GaN would cause a dramatic increase of this issue. Due to the high frequencies applied to the winding system with a voltage step, a nonlinear voltage distribution occurs, because the impedance of the series inductances is relatively large compared to the capacitive impedance [1], [24]. This results in an unbalanced voltage stress along the coils of a phase, with higher stress for the first coils near to the phase terminal. For higher inhomogeneous voltage distribution the probability of ∗∗partial discharges (PD's) rises.

The proposed monitoring method for the insulation state estimation is based on analysis of the transient current reaction as a result of voltage step excitation separately in every phase. The high *dv/dt* of the voltage steps and the impedance mismatch of the supply cables between inverter and machine cause a transient overvoltage at the machine terminals. A transient is also observable in the current transducer's response and the characteristic depends beside the switching transition—common mode or differential mode [25], [26], on the condition of the motor's insulation system. According to the aforementioned analyzes in Section II, the parasitic components of a winding system, e.g., turn-to-turn, winding-to-ground capacitances etc., significantly change after a specific number of aging cycles have been applied. These changes can be analyzed with the observation of the transients.

In this paper the degradation of the insulation system for the 1.4 MW induction machine is emulated with a capacitor placed parallel to the winding system implemented at a special three phase induction machine equipped with taps. In Fig. 8, two current responses measured in phase L1, after a voltage step is applied with the inverter, starting all phases at the lower dc-link voltage followed by a transition of the corresponding inverter lag by turning OFF the low side transistor and turn ON the high side one.

The solid blue trace depicts a healthy machine and the dashed green the same machine with a capacitor placed parallel to the first coil of phase L1. The capacitor with a size of 3 nF parallel to the first coil of phase L1 emulates a change of the parasitic winding capacitances and influences the shape of the high-frequency oscillation. The total winding-to-ground capacitance is estimated with 63nF. According to studies in this paper and referenced in the paper, e.g., [18] and [19], change in capacitance over lifetime is around 20% to 25% of initial value what would result in around 12 nF to 16 nF for the whole machine

TABLE I
TEST BENCH DETAILS

DC linkvoltage	f_S	Resolution(n-bit)
440 V	120 MS/s (1MS/s*)	16 (10*)

* minimum recommended

winding. To simulate also small values of insulation degradation, the range of capacitance values used in the measurements was between 330 pF and 3 nF.

The ringing decays within a few micro second followed by the typical inductive behavior. The recorded signal $i(t)$ is a superposition of a linear current rise (due to the inductive properties of the machine) and transient (high-frequency part) i_{trans}, described in the following equation:

$$i\left(t\right) = i_{\mathrm{trans}}\left(t\right) + \frac{1}{L}\int_{-\infty}^{t} u\left(t\right) dt \tag{1}$$

The current slope depends on machine inductance and inherent asymmetries, e.g., slotting or saturation, and is always removed in the following investigations to ensure that the rotor position has no influence on the method.

The industrially applied standard hall-effect-based closed loop current transducers (*di/dt*>50 A/μs) were placed in a shielded sensor box and connected with shielded cables to prevent disturbing influences. The current traces were sampled with a sampling rate and resolution of 120 MS/s and 16 bit (for practical realization a reduction down to 1 MS/s and 10 bit using special signal processing means was verified without significant loss in detection sensitivity, see [27]).

The measurements are made with lower dc-link voltage (440 V), as intended for a real traction motor, where the dc-link voltage usually is around (2.8 kV). For the rated voltage of 2.8 kV the currents will be about 6.4 times higher. A short summary about parameters of the test bench is given in Table I.

The characteristics of the deviation in the shape of both transients are analyzed in the frequency domain. The scheme of the signal processing is depicted in Fig. 9. The accurate switching instant has to be determined and by applying a simple rectangular windowing function the time domain data are transferred with Fourier analysis into the frequency domain.

Due to the dependency of the affected frequency range on different parameters, e.g., machine size or capacitor position, a wide frequency range up to 500 kHz is suitable for this type of machine to detect a deviation between healthy machine state and emulated insulation degradation. If the degradation affects the whole phase, the degradation is observable over a wide range from 50 kHz to 500 kHz. In case of a single coil or turn–turn degradation the range can be quantified from 100 kHz to 200 kHz. Therefore, the whole frequency range is analyzed and is included in the calculation of an indicator, denoted as ISI in the following. This indicator is based on the calculation of the RMSD calculated from the difference of the healthy machine state spectrum and spectra of further measurements. With the following equation, the indicator for the actual machine state is

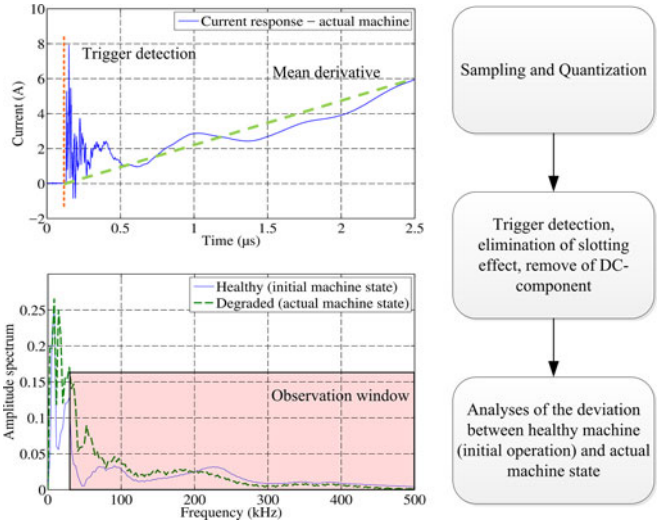

Fig. 9. Scheme of signal processing.

calculated:

$$\begin{aligned} \mathrm{ISI}_p &= \mathrm{RMSD}_p\left(x_1, x_2\right) \\ &= \sqrt{\frac{\sum_{i=1}^{n}\left(Y_{\mathrm{ref},p}\left(f_i\right) - Y_{\mathrm{con},p,k}\left(f_i\right)\right)^2}{n}}. \end{aligned} \tag{2}$$

In order to ensure statistical interpretation of the data, one machine state is represented by a high number of consecutive measurements. These measurements are taken in a sequence and in this paper the number was set to 100 measurements. For the representation of the healthy machine state a reference spectrum is formed out of the 100 different single spectra with the mathematical operation of the median, denoted with $Y_{\mathrm{ref},p}$. The index p identifies the investigated phase. At each discrete frequency point f_i all amplitude values of the single spectra are sequentially sorted and the median for every *ith* frequency point is used for the reference spectrum. The second variable, denoted with $Y_{\mathrm{deg},p,k}$ represents the amplitude spectrum of the emulated insulation degradation measurement. In this case, the median operation is not applied and the index k represents the consecutive number of the repeated measurement. The variable n depends on the observed frequency range from 50–500 kHz.

Since the proposed method is a comparative method, the focus is therefore on the high degree of reproducibility of the measurements for the machine states. Thus, in Fig. 10 the spectra of the transient part of the preprocessed current responses are depicted and in the enlarged subfigure, the minimum and maximum values and the standard deviation $\pm\sigma$ of the spectral components are shown. As can be seen the variance of the data points in the spectrum of the 100 recorded current responses is very low and high reproducibility is still given. The minimum system requirements and investigations on additional disturbing influences (e.g., cabling length, temperature, and moisture) are described in [28]–[31].

The resulting indicator values for the healthy and degraded machine state and further investigated degradation scenarios

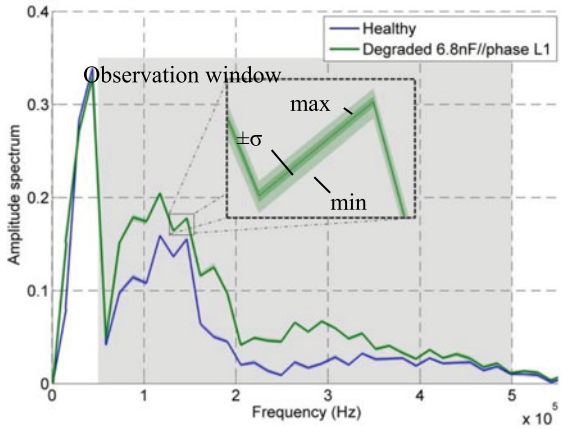

Fig. 10. Spectra of 100 healthy current signals (solid blue) and emulated insulation degradation (solid green), with $\pm\sigma$ standard deviation and minimum/maximum deviation.

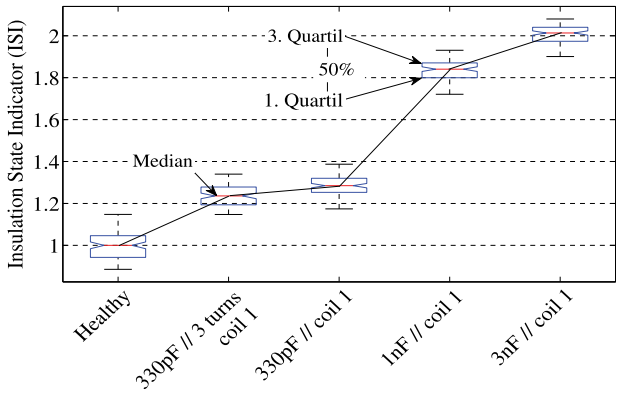

Fig. 11. Box plots of the insulation state indicator for different machine conditions compared with reference measurement (healthy condition).

are depicted in Fig. 11. An increase in the indicator by use of larger capacitance values can be equated with an increasingly deteriorated insulation, and this is equivalent to a change in the capacitance of the winding. The label "*Healthy*" means that a second measurement of this machine state is given and the direct comparison of these two measurements results in a value that is not equal to zero. This has to be interpreted as a kind of variance of the measurement system. All values are scaled to this factor and as a consequence all values above the value 1 indicates a deterioration of the insulation state.

To emulate incipient insulation defects a capacitor with 330 pF was placed parallel to three of five turns ("*denoted 330 pF // 3 turns coil 1*") of the first form-wound coil in phase L1. The total winding to ground capacitance is about 63 nF. The expected capacitance change is indicated with about 20–25% according to studies of different authors, e.g., [18] and [19]. In Fig. 11, the indicators show a monotonic increasing tendency for the increasing emulated insulation degradation severity with increasing capacitor values.

With the so called "box plot" representation the distribution of the resulting indicator values is given. With the red line in the center of a box plot, the median of 100 consecutive measurements is shown and the lower and upper limit of the blue box indicates the 25th, respectively, 75th percentile. With no overlapping, it can be concluded that with 95% confidence the medians differ between the analyzed machine conditions. In the investigated scenarios, all machine conditions are clearly separable from the healthy machine state.

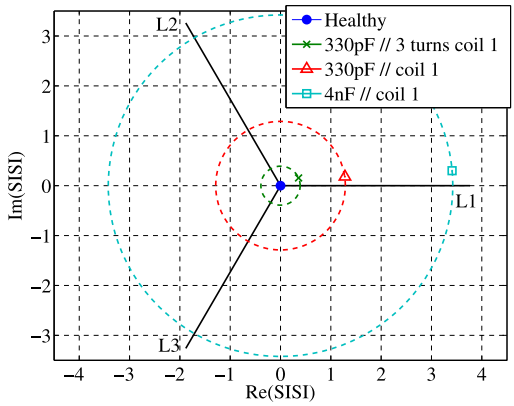

Fig. 12. SISI for different investigation conditions.

Additionally, to detect the affected phase in which the insulation degradation occurs, the linear combination of the previous calculated ISI-phase values can be defined in the following equation, denoted with SISI:

$$\mathrm{SISI} = \mathrm{ISI}_{L1} + \mathrm{ISI}_{L2} * e^{\frac{j2\pi}{3}} + \mathrm{ISI}_{L3} * e^{\frac{j4\pi}{3}}. \qquad (3)$$

With the linear combination only asymmetrical changes are detected whereas symmetrical ones, e.g., are eliminated as these would lead to zero-sequence components. In Fig. 12, the spatial representation of the investigated degradation scenarios are given and the assignment of degradation to the corresponding phase is possible. The distance between origin of the plane and the locus of the SISI pointer represents the severity of the insulation deterioration.

Regarding the implementation in the target system the insulation state evaluation can be performed each time the train is leaving a station and blocking of inverter switching commands is over. The switching patterns by the inverter to test all three phases are applied by communication with the control unit of the motor. Calculation results, time stamps, temperatures, time signals (current signals,..) will be stored in an external memory for further analysis. Generally, the process of insulation deterioration is slowly developing. In order to obtain enough ISI data points for a trend analysis, it is thus sufficient to choose the time interval for conducting the proposed measurement to once every week or even month before starting service. In addition, temperature values are measured for comparison purpose to stay within a defined margin, because influence due to temperature variations could not be excluded, see Section III "*B – Influence of temperature.*"

A. ISI of the Formette

In this section, the approach of the insulation monitoring method based on the voltage step excitation response of the current transducers is tested at the formette type I. With a step

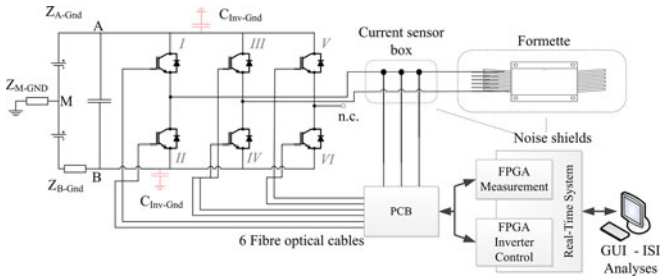

Fig. 13. Schematic overview of the test-bench.

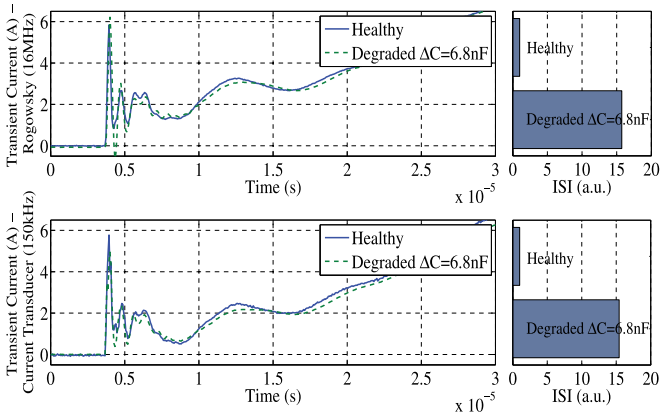

Fig. 14. Comparison between current signal evaluation between Rogowsky coil and current transducer.

voltage the system is stimulated with a broadband frequency range instead of stimulation with single frequency and again the high-frequency current response is recorded using the current transducer signal. After each thermal exposure the current transducer response is analyzed. The test bench is schematically depicted in Fig. 13 with the formette connected to an IGBT-voltage source inverter, which is fed by a constant dc-link voltage of 440 V. Three closed loop compensating transducers with bandwidth specifications of up to 150 kHz are placed in the current transducer box to observe the variance between the transducers. With a Rogowski coil (specified bandwidth of 16 MHz) the results are verified using an oscilloscope. To increase the precision of a measurement, the transducers and specimen are placed into shielded boxes to prevent disturbing influences.

Due to the special construction of the closed loop compensating transducers with its Hall-generator and the secondary coil acting as compensation coil, the bandwidth is significantly extended and the response time of the sensor is improved. At lower frequencies the transducer operates using the Hall-generator. At higher frequencies the secondary coil operates as a current transformer significantly extending the bandwidth and reducing the response time of the transducer. This topic was also verified by measurements carried out by the current transducer manufacturer company. Absolute accuracy of the transducers is reduced, however reproducibility is guaranteed even in megahertz range. Fig. 14 depicts a measured reference current response using Rogowsky coil (16 MHz) (upper traces) and current transducer (150 kHz) (lower traces). Both sensors have been tested for the

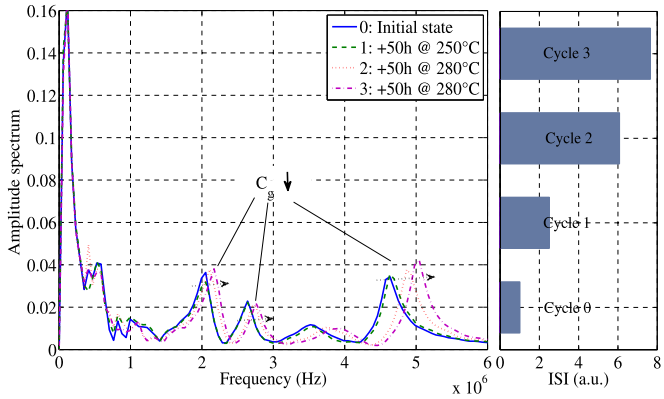

Fig. 15. Spectra of the measured current responses at states 0–3.

healthy configuration, as well as emulated insulation degradation $\Delta(C = 6.8\ \text{nF})$.

As can be seen in the calculated ISI values both sensors deliver comparable sensitivity to the emulated changes of the winding insulation. Though the current transducer has a higher signal variance, the emulated degradation of the insulation is clearly detectable and separable.

The spectra of the recorded transient responses of the formette states as described in Section II-C are depicted in Fig. 15. The blue trace, denoted with "*0: initial state*" depicts the trace for the initial unaged state of the winding system. The state "*1*" is defined with a heat exposure duration of 50 h and 250 °C and for state "*2*" and state "*3*" the temperature is increased to 280 °C. After each state, the global capacitance C_g of the formette, formed by the turn-to-turn, winding-to-ground capacitance, etc., (cf. Fig. 6) changes and a tendency of shifted resonance peaks towards higher frequency values is visible.

All states are clearly separable and the indicators show a monotonic increasing tendency for increasing severity of insulation degradation. The effects of the shifted resonance peaks are in accordance to (4), with increasing frequency at decreasing capacitance.

The circuit model shows the parallel C_p and R_p in addition to the series connected R_S and L_S configuration, which depicts the capacitive current flowing through the insulation and the power dissipated in the insulation and the conductor. The loss of the capacitor is neglected relative to the loss of the coil. This is a simplified model of the arrangement, since the electrical properties changes between being capacitive and inductive at higher frequencies.

$$f_r \sim 1/2\pi \sqrt{\left(\frac{1}{LC} - \frac{R^2}{L^2}\right)} \qquad (4)$$

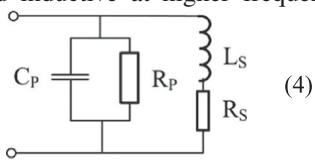

In Fig. 16, the stator slot cross section with inserted form-wound coil and indicated parasitic capacitances (turn-to-turn capacitance C_{t-t}, coil-to-coil C_{c-c}, groundwall capacitance $C_{w-\text{gnd}}$, and changes due to aging indicated by ΔC) emphasize the changes of the initial values. Due to operation under harsh conditions and the influence of several stresses, the

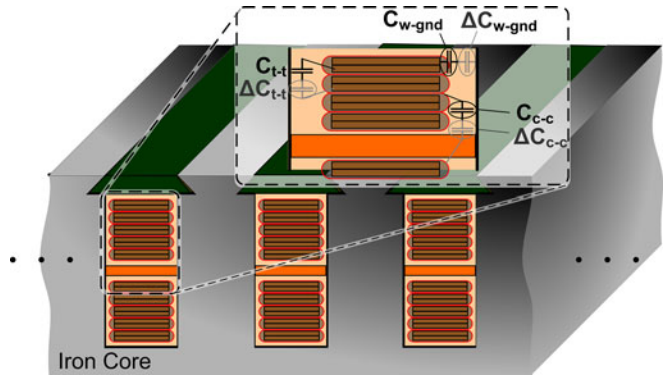

Fig. 16. Stator slot cross section with inserted form-wound coil and indicated parasitic capacitances.

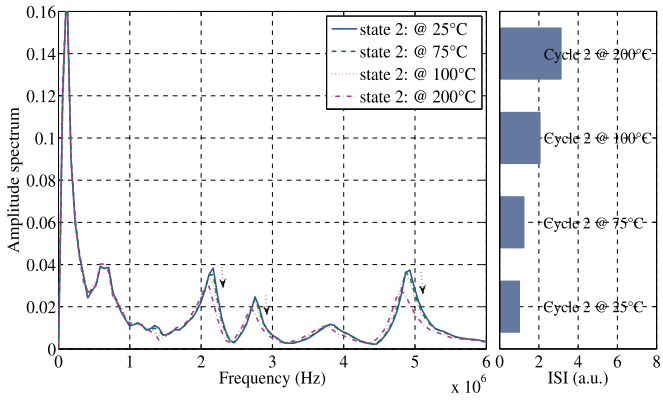

Fig. 17. Influence of temperature (25–200 °C) on current responses spectra measured at state 2.

insulation material is deteriorated, for instance due to PD resulting in changes of the chemical bonds. By using a simple capacitive voltage divider, the single capacitances are calculated like a parallel plate capacitor with the permittivity $\varepsilon = \varepsilon_r \varepsilon_0$, the permittivity of the free space ε_0 and relative permittivity ε_r (dielectric constant) of the material in combination with the geometrical factors cross-sectional area and thickness of insulation material. The dielectric constants of the insulation material and air, which can be encased in voids, are different by a factor of 4. However, due to sparks the occurrence of residual products, through rupture of chemical bonds is possible and the classification in air and insulation material is not feasible. Additionally, since the geometrical properties cannot be accurately determined, the model is only a rough approximation.

B. Influence of Temperature

In Fig. 17, the spectra of the formette after state "*2*" at different temperature levels are depicted. The measurements are conducted during the cooling process to analyze the influence of temperature on the results. Four different temperatures 200, 100, and 75 °C and ambient temperature 25 °C are analyzed. From the curves the influence of the temperature on the proposed monitoring method is visible. Only the magnitude in the spectra has changed and the second resonance peak is mainly

(a)

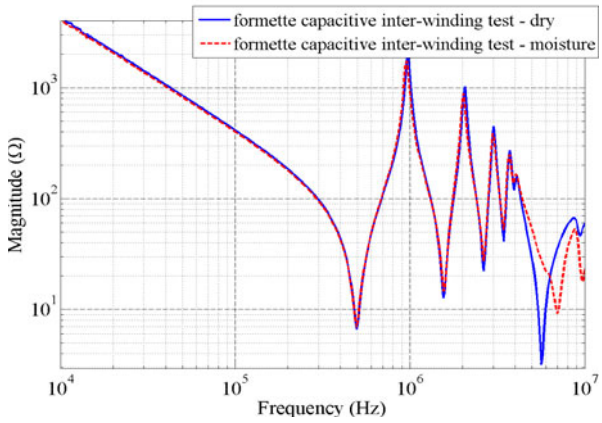

(b)

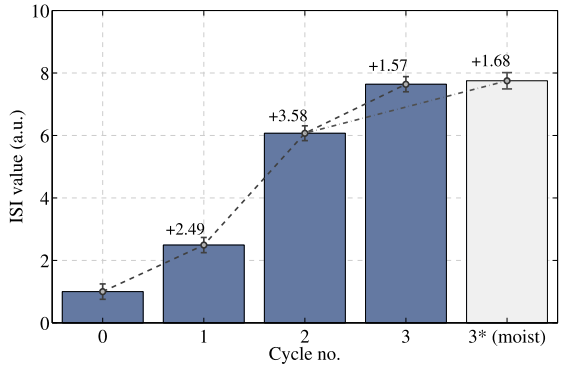

(c)

Fig. 18. (a) Formette after humidity chamber (b) frequency characteristic measurement of the formette in dry and moist state (c) calculated ISI values for all aging states (0–3) and comparison of dry and moist state.

decreasing with the temperature in contrast to the shift of the resonance caused by a decreasing capacitance value. At higher temperatures the resistance values are mainly influenced and as a consequence the damping of the system.

The indicators in the right subfigure show clear increase and in worst case with 200 °C winding temperature of the fromette, a value of 1.64 a.u. is reached, which corresponds more than the deviation after the state "*1*" with a ΔC of approximately 200 pF. Due to the simple algorithm of the RMSD calculation this difference is not considered and thus the temperature or more precisely the change caused by temperature is not negligible. In order to increase the reliability and to prevent interference

caused by the influence of temperature, the authors recommend that the measurements for the estimation of the insulation state are always compared at a similar temperature level. With the temperature sensor of the motor, the temperature has to be stored together with the measurement data. A comparison and calculation of the fault indicator within a deviation of approximately $\pm 10\ ^{\circ}\mathrm{C}$ of both measurements is recommended.

C. Influence of Moisture

In the last section the influence of moisture is analyzed. In Fig. 18(a) the formette after the humidity chamber is depicted. To analyze the influence of moisture on the accuracy of the method all tests are repeated in this state and compared to the measurements after drying of the formette.

In Fig. 18(b) the frequency sweep mode from 10 to 10 MHz show deviations in the higher frequency range above 1 MHz between the formette measurement in a dry state (solid blue) and moisture exposure formette (dashed green). With respect to the values of the dissipation factor and capacitance from Figs. 5 and 6 and further voltage exposure tests the state of the insulation can be considered as not critical. The low impact of humidification in these tests can be explained by the fact that a low test voltage is used and that the number of cracks in the insulation system is low and delamination has not occurred up to this state.

In Fig. 18(c) the calculated indicator values ISI are shown at aging state 0–3 including the comparison of the last state in dry and moist. With focus on last mentioned scenarios state "3" and state "3$*$ (moisture)," the influence of the moisture on the results is not observable, although the variance has slightly increased at state "3$*$ (moisture)". Both the time signals of the transient current response as well as the spectra show no clear deviation.

IV. Conclusion

Investigations regarding accelerated ageing of a medium voltage insulation system of single form wound coils and a formette are presented. Dissipation factor and capacitance measurement show clearly the change of the insulation characteristic during aging and allow the qualification of the severity of the reduced insulation strength. These preliminary results enable the selection of conditions for further formette tests according to the IEEE standard 1776-2008. With the knowledge of the possible value of the capacitance changes of up to 20–25% from the initial value, further investigations of the proposed insulation monitoring technique for inverter fed traction motors are possible. The technique is based on the evaluation of the current transients after step voltage excitation applied by the inverter. The characteristics of the transients are mainly influenced by the motor's parasitic capacitances. The insulation degradation is always linked with a change of this capacitance that is considered the dominant parameter for insulation health state evaluation. After special signal processing the transient information is analyzed in the frequency domain by applying the fast Fourier transformation. Based on a comparative method the deviation between reference measurement at initial operation of the motor and later in-service measurements give evidence about the insulation state. Through measurements on a 1.4 MW induction machine and different emulated insulation degradation scenarios the applicability of the proposed method is verified. Additionally the method is tested on the formette after every applied thermal cycle and delivers results suitable for the insulation state estimation.

Acknowledgment

The authors would like to thank M. Joerg, Head of RoQ_P-CoE2, and his team at Bombardier Transportation Switzerland Ltd., and E. Moser, L. Pfeil, G. Harasleben, and R. Sieder in the RoQ_Drives Department, Bombardier Transportation Austria GmbH, for their support. Special thanks from the authors go to M. Bazant, Head of RoQ_Drives Product Development and Management, Bombardier Transportation, for generous support, all the feedback over several years, and for research/development funding. Further thanks go to the colleagues from ISOVOLTA Austria Company and TUVienna, and LEM - Company (especially W. Teppan and J. Burk for the cooperation).

References

[1] G. C. Stone, E. E. Boulter, I. Culbert, and H. Dhirani, *Electrical Insulation for Rotating Machines*, Piscataway, NJ, USA: IEEE Press, 2004.

[2] I. Culbert, H. Dhirani, and G.C. Stone, "Handbook to assess the insulation condition of large rotating machines," *EPRI Power Plant Elect. Ref. Ser.*, vol. 16, 1989.

[3] K. Younsi *et al.*, "On-line capacitance and dissipation factor monitoring of ac stator insulation," *IEEE Trans. Dielect. Elect. Insul.*, vol. 17, no. 5, pp. 1441–1452, Oct. 2010.

[4] *IEEE Recommended Practice for Measurement of Power Factor Tip-Up of Electric Machinery Stator Coil Insulation*, IEEE Standard 286-2000, pp. 1–36, 2000.

[5] *IEEE Recommended Practice for Testing Insulation Resistance of Electric Machinery - Redline*, IEEE Standard 43-2013 (Revision of IEEE Std 43-2000) - Redline, pp. 1–75, 2014.

[6] J. Ahola, V. Särkimäki, A. Muetze, and J. Tamminen, "Radio-frequency-based detection of electrical discharge machining bearing currents," *IET Elect. Power Appl.*, vol. 5, no. 4, pp. 386–392, 2011.

[7] S. Ait-Amar and D. Roger, "Prospective method for partial discharge detection in large AC machines using magnetic sensors in low electric field zones," *IET Int. Conf. Comput. Electromagn.*, vol. 5, no. 4, pp. 386–392, 2011.

[8] H. A. Toliyat, S. Nandi, S. Choi, and H. Meshgin-kelk, *Electric Machines: Modeling, Condition Monitoring, and Fault Diagnosis*. Boca Raton, FL, USA: CRC Press, 2012.

[9] J. Yang, J. Cho, S. B. Lee, J.-Y. Yoo, and H. D. Kim, "An advanced stator winding insulation quality assessment technique for inverterfed machines," *IEEE Trans. Ind. Appl.*, vol. 44, no. 2, pp. 555–564, Mar./Apr. 2008.

[10] F. Perisse, D. Mercier, E. Lefevre, and D. Roger, "Robust diagnostics of stator insulation based on high frequency resonances measurements," *IEEE Trans. Dielect. Elect. Insul.*, vol. 16, no. 5, pp. 1496–1502, Oct. 2009.

[11] R. M. Tallam, T. G. Habetler, and R. G. Harley, "Stator winding turn-fault detection for closed-loop induction motor drives," in *Proc. IEEE 37th IAS Annu. Meeting Conf. Rec. Ind. Appl. Conf.*, Pittsburgh, PA, USA, 2002, vol. 3, pp. 1553–1557.

[12] S.-B. Lee, J. Yang, K. Younsi, and R. M. Bharadwaj, "An online groundwall and phase-to-phase insulation quality assessment technique for ac machine stator windings," *IEEE Trans. Ind. Appl.*, vol. 42, no. 4, pp. 946–957, Jul./Aug. 2006.

[13] S. Grubic, J. Restrepo, and T.G. Habetler, "Online surge testing applied to an induction machine with emulated insulation breakdown," *IEEE Trans. Ind. Appl.*, vol. 49, no. 3, pp. 1358–1366, May/Jun. 2013.

[14] P. Neti and S. Grubic, "Online broadband insulation spectroscopy of induction machines using signal injection," in *Proc. IEEE Energy Convers. Congr. Expo.*, 2014, pp. 630–637.

[15] T. Ghanbari, "Autocorrelation function-based technique for stator turn-fault detection of induction motor," *IET Sci., Meas. Technol.*, vol. 10, no. 2, pp. 100–110, 2016.

[16] J. Ramírez-Niño, A. Pascacio, R. Mijarez, and J. Rodriíguez-Rodriíguez, "On-line fault monitoring system for hydroelectric generators based on spectrum analysis of the neutral current," *IET Gener., Transmiss. Distrib.*, vol. 9, no. 16, 2015.

[17] A. Bellini, F. Filippetti, C. Tassoni, and G.-A. Capolino, "Advances in diagnostic techniques for induction machines," *IEEE Trans. Ind. Electron.*, vol. 55, no. 12, pp. 4109–4126, Dec. 2008.

[18] M. Farahani, E. Gockenbach, H. Borsi, K. Schaefer, and M. Kaufhold, "Behavior of machine insulation systems subjected to accelerated thermal aging test," *IEEE Trans. Dielect. Elect. Insul.*, vol. 17, no. 5, pp. 1364–1372, Oct. 2010.

[19] M. Farahani, H. Borsi, and E. Gockenbach, "Study of capacitance and dissipation factor tip-up to evaluate the condition of insulating systems for high voltage rotating machines," *Elect. Eng.*, vol. 89 no. 4, pp. 263–270, 2007.

[20] F. Perisse, P. Werynski, and D. Roger, "A new method for AC machine turn insulation diagnostic based on high frequency resonances," *IEEE Trans. Dielect. Elect. Insul.*, vol. 14, no. 5, pp. 1308–1315, Oct. 2007.

[21] *IEEE Recommended Practice for Thermal Evaluation of Unsealed Or Sealed Insulation Systems for AC Electric Machinery Employing Form-Wound Pre-Insulated Stator Coils for Machines Rated 15 000 V and Below*, IEEE Standard 1776-2008, 2009.

[22] N. Oswald, P. Anthony, N. McNeill, and B.H. Stark, "An experimental investigation of the tradeoff between switching losses and EMI generation with hard-switched all-Si, Si-SiC, and All-SiC device combinations," *IEEE Trans.Power Electron.*, vol. 29, no. 5, pp. 2393–2407, May 2014.

[23] N. Lahoud, J. Faucher, D. Malec, and P. Maussion, "Electrical aging of the insulation of low-voltage machines: Model definition and test with the design of experiments," *IEEE Trans. Ind. Electron.*, vol. 60, no. 9 pp. 4147–4155, Sep. 2013.

[24] B. K. Gupta, B. A. Lloyd, G. C. Stone, S. R. Campbell, D. K. Sharma, and N. E. Nilsson, "Turn insulation capability of large AC motors part 1 - surge monitoring," *IEEE Trans. Energy Convers.*, vol. EC-2, no. 4, pp. 658–665, Dec. 1987.

[25] G. Skibinski, R. Tallam, R. Reese, B. Buchholz, and R. Lukaszewski, "Common mode and differential mode analysis of three phase cables for PWM AC drives," in *Proc. 41st IAS Annu. Meeting Conf. Rec. IEEE Ind. Appl. Conf.*, Tampa, FL, USA, 2006, pp. 880–888.

[26] B. Mirafzal, G. L. Skibinski, R. M. Tallam, D. W. Schlegel, and R. A. Lukaszewski, "Universal induction motor model with low-to-high frequency-response characteristics," *IEEE Trans. Ind. Appl.*, vol. 43, no. 5, pp. 1233–1246, Sep./Oct. 2007.

[27] C. Zoeller, M. A. Vogelsberger, J. Bellingen, P. Nussbaumer, and T. M. Wolbank, "Investigation of sampling frequency and jitter effects on transient current signal evaluation for insulation condition monitoring," in *Proc. 17th Euro. Conf. Power Electron. Appl.* , Geneva, Switzerland, Sep. 2015, pp. 1–9.

[28] P. Nussbaumer, T.M. Wolbank, and M.A. Vogelsberger, "Sensitivity analysis of insulation state indicator in dependence of sampling rate and bit resolution to define hardware requirements," in *Proc. IEEE Int. Conf. Ind. Technol.* , 2013, pp. 392–397.

[29] P. Nussbaumer, T.M. Wolbank, and M.A. Vogelsberger, "Separation of disturbing influences on induction machine's high-frequency behavior to ensure accurate insulation condition monitoring," in *Proc. 28th Annu. IEEE Appl. Power Electron. Conf. Expo.*, 2013, pp. 1158–1163.

[30] C. Zoeller, M.A. Vogelsberger, P. Nussbaumer, and T.M. Wolbank, "Insulation monitoring of three phase inverter-fed AC machines based on two current sensors only," in *Proc. Int. Conf. Elect. Mach.*, 2014, pp. 1901–1907.

[31] C. Zoeller, M. A. Vogelsberger, R. Fasching, W. Grubelnik, and Th.M. Wolbank, "Evaluation and current-response based identification of insulation degradation for high utilized electrical machines in railway application", in *Proc. 2015 IEEE 10th Int. Symp. Diagno. Elect. Mach. Power Electron. Drives*, 2015, pp. 266–272.

Clemens Zöller received the M.Sc. degree in power engineering from the Vienna University of Technology, Vienna, Austria, in 2013.

He is currently a Project Assistant with the Institute of Energy Systems and Electrical Drives, Vienna University of Technology, where he is engaged in several industrial and scientific projects with focus on electrical drives. His research interests include fault detection, condition monitoring, and sensorless control of inverter-fed ac machines.

Markus A. Vogelsberger received the Dipl. Ing. (Hons.) and Dr. Techn/Ph.D. (Hons.), degrees in electrical engineering from the Vienna University of Technology (TU-Vienna), Vienna, Austria, in 2004 and 2009, respectively.

He was a Scientific Research Assistant at the Institute of Electrical Drives and Machines, TU-Vienna, where he has been engaged in several industrial and scientific research and development (R&D) projects. He was at the Georgia Institute of Technology University, Atlanta, GA, USA, for study and research activities in 2006 and 2008, respectively. Since 2011, he has been with Bombardier Transportation, Vienna, as the R&D Project Lead in the Rolling Stock Equipment (RoQ)-Drives Engineering Department. His research interests include traction motors, power electronics, drives topics, and multidisciplinary R&D projects. His current focus is on the research and management of the high innovative condition monitoring and speed sensorless drives strategies for ac traction drives, and the interdisciplinary and multiobjective R&D project on thermo-efficient traction.

Robert Fasching received the M.Sc. degree in power engineering from the Graz University of Technology, Graz, Austria, in 2014.

Since 2014, he has been with Isovolta AG, Wiener Neudorf, Austria, as an Application Engineer. His research interests include the study and application of dielectrics of insulation systems in industrial, commercial, and power system equipment.

Werner Grubelnik (M'04) was born in Trofaiach, Styria, in 1971. He received the graduate degree in electrical engineering from the Technical University Graz, Graz, Austria, in 2002.

Since 2002, he has been with Isovolta AG, Wiener Neudorf, Austria, where he is responsible for the field of application engineering. He has published several papers on various conferences in the last 10 years.

Thomas M. Wolbank (M'99) received the graduate degree in industrial electronics, the Dr. techn. degree, and the habilitation degree in electrical drives from the Vienna University of Technology, Vienna, Austria, in 1989, 1996, and 2004, respectively.

He is with the Department of Energy Systems and Electrical Drives, Vienna University of Technology. He has co-authored approximately 150 papers in refereed journals and international conferences. His research interests include saliency-based sensorless control of ac drives, dynamic properties and condition monitoring of inverter fed machines, and transient electrical behavior of ac machines.